Econ. Environ. Geol.
Vol. 31, No. 5, p. 389-398, 1998.

Hydrothermal Au-Ag Mineralization of the Oknam Mine in the Northern Sobaegsan Massif*

Seong-Taek Yun, Se-Jung Chi***, Chil-Sup So** and Chul-Ho Heo****

ABSTRACT : The Au-Ag deposit of the Oknam mine occurs as gold-silver-bearing rhodochrosite veins in biotite schist and phyllite of the Precambriam Yulri Group. Five stages of ore deposition are recognized, each showing a definite mineral assemblage. General mineral parageneses in veins (stage III) associated with gold and silver vary inwardly from the vein margin: arsenopyrite + pyrite ⇒ sphalerite+chalcopyrite+galena+gold ⇒ galena+Ag-bearing minerals. Fluid inclusion data indicate that temperature and salinity of ore fluids overally decreased with time: 345°~240°C and 3.4~7.8 wt. % NaCl equiv during stage I (quartz vein mineralization), 313°~207°C and 2.3~8.7 wt.% NaCl equiv during manganese-bearing carbonate stages (II and III), and 328°~213°C and 3.6~5.4 wt.% NaCl equiv during stage IV (quartz vein mineralization). The ore fluids probably evolved through repeated pulses of boiling and later mixing with cooler and more dilute meteoric waters. Fluid inclusion data and geologic arguments indicate that pressures during the mineralization were in the range of 90 to 340 bars. Gold occurs as silver-rich electrums (21 to 29 atom.% Au) and was deposited at temperatures between 300° and 240°C. Thermochemical calculations suggest that gold was deposited as a combined result of increase in pH and decreases in temperature, fs_2 and fo_2.

INTRODUCTION

In South Korea, three major types of gold-silver mineralization have been documented which display a consistent relationship among age, depth, water-to-rock ratio (degree of meteoric water involvement), and Au/Ag ratio (Shelton *et al.*, 1988; So *et al.*, 1989). These are: Jurassic, gold-rich mesothermal deposits; Early Cretaceous, "Korean-type" gold-silver deposits; and Late Cretaceous, more silver-rich epithermal deposits.

Mesothermal gold deposits associated with Jurassic "Daebo" granites are characterized by high Au/Ag ratios (5:1 to 8:1), and were formed at high temperatures (300° to 370°C) in response to unmixing of CO_2-rich fluids at depths of >4.5 km. The "Korean-type" gold-silver deposits associated with Early Cretaceous granites have high Au/Ag ratios (1:3 to 2:1), and were formed at temperatures near 270°C under depths near 1 km. Epithermal gold-silver deposits associated with Late Cretaceous to Tertiary "Bulgugsa" granites are characterized by lower Au/Ag ratios (1:10 to 1:200) and more abundant and complex sulfide mineralization, and were formed at temperatures of <240°C under depths of <1 km.

Within the Taebaegsan metallogenic belt, located about 220 km south-east-east of Seoul, numerous hydrothermal metallic ore deposits occur. The studies on the representative deposits within this belt are as follows: Janggun Mn-Pb-Zn-Ag (Imai, Lee, 1980; Kim, 1986; Lee *et al.*, 1990), Shinyemi Zn-Pb (Kim, Nakai, 1980; Kim *et al.*, 1981; Yang *et al.*, 1993), Yeonhwa Zn-Pb (Yun, 1979; Koh *et al.*, 1992; So *et al.*, 1993). However, the studies on gold-silver mineralization in this belt are relatively scarce. The Oknam mine (latitude 36°53'N, longitude 129°6'E) represents a characteristic hydrothermal Au-Ag-Mn mineralization in the Taebaegsan belt, and consists of rhodochrosite veins accompanying economic concentrations of gold and silver. General ore grades at Oknam are 0.2~3.6 g/t Au and 247~2,716 g/t Ag.

The aims of this study are to document the nature and physicochemical conditions of hydrothermal Au-Ag mineralization at Oknam, and to elucidate the origin of hydrothermal fluids and the mechanism of gold deposition in rhodochrosite vein.

GEOLOGY

The Oknam mine area is located within northeastern part of the Precambrian Sobaegsan Massif, and occupies about 5 km northeast of the famous Janggun Pb-Zn-Ag-Mn mine. Geology of the mine area

* This study was supported by the academic research fund of Ministry of Education, Republic of Korea

** Department of Earth and Environmental Sciences, Korea University, Seoul 136-701, Korea, E-mail: styun@kuccnx.korea.ac.kr

*** Geochemistry Division, Korea Institute of Geology, Mining and Materials, Taejeon 305-350, Korea

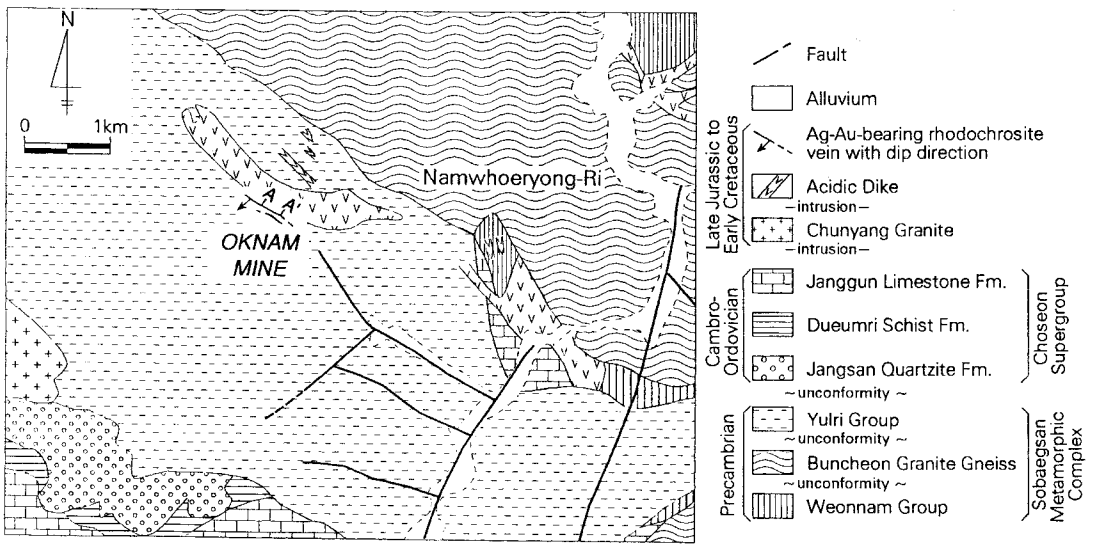

Fig. 1. Geologic map of the Oknam Au-Ag mine area (modified after Kim *et al.*, 1962). The line A-A′ indicates the location of cross sections shown in Fig. 2.

is mainly underlain by metamorphic rocks of the Weonnam and Yulri Groups, and Buncheon granitic gneiss. The Cambro-Ordovician metasedimentary rocks of the Choseon Supergroup, and Late Jurassic to Early Cretaceous igneous rocks also occur in the area (Fig. 1).

The Weonnam Group, the bottom sequence of the mine area, consists of granitic gneiss and porphyroblastic gneiss. The Buncheon granitic gneiss distributed in the northeastern part of the study area unconformably overlies the Weonnam Group, and shows a gradational contact with the Hyundong Schist Complex out of the study area. It shows poor schistosity. Quartz with myrmekitic and mortar textures is strongly elongated parallel to the foliation. Available radiometric ages by Rb/Sr methods on the Buncheon granitic gneiss are 2,107 m.y. (Choo, Kim, 1985) and 1,400 m.y. (Ueda, 1968). The Yulri Group overlies unconformably the Weonnam and Buncheon groups, and consists of pelitic and psammitic metasedimentary rocks. The Group in the mine area includes biotite-quartz-andalusite schist, chlorite schist, biotite-sillimanite schist, and phyllite. They are thinly interbedded with cross-bedding.

The Choseon Supergroup ($\leq$2.5 km in thickness) in the mine area unconformably overlies the Yulri Group, and consists of the Jangsan Quartzite Formation, Dueumri Schist Formation, and Janggun Limestone Formation, in ascending order. The Jangsan Quartzite Formation ($\leq$300 m thick) is light to dark gray in color and contains elongated quartzite pebbles ($\leq$10 cm in diameter) parallel to bedding planes in the bottom of beds. The Dueumri Schist Formation overlies conformably the Jangsan Quartzite Formation, and consists mainly of dark gray phyllite interbedded with thin crystalline limestone. The Janggun Limestone Formation ($\leq$800 m thick) conformably overlies the Dueumri Schist Formation, and dominantly comprise massive pale gray limestone with intercalations of silicified limestone, crystalline limestone and dolomitic limestone. In the upper parts of the formation, thin greenish phyllite beds are alternated with limestone.

Late Jurassic to Early Cretaceous igneous rocks intrude the rocks described above, and consist of the Chunyang Granite and acidic dikes. The Chunyang Granite occurs about 3 km west of the Oknam mine. Dikes of porphyrite, quartz porphyry, granite porphyry and pegmatite are ubiquitous in the mine area. Their directions are usually parallel to the N-W-trending fault system.

ORE VEINS

Two major Ag-Au-bearing rhodochrosite veins and several barren quartz or carbonate veins occupy the fault shear zones (each $\leq$3 m thick) in biotite schist and phyllite of the Yulri Group (Fig. 1). These veins preferentially occur at the footwall side of the fault shear zone with fault gouge. They (each several hundreds meters long) strike N45°W and dip 50°~80°SW. Pegmatite dikes ($\leq$0.3 m thick) often occur parallel to the veins. Barren quartz veins vary in thickness from 0.01 to 0.15 m (avg. = 0.05 m), and show repeated pinching and swelling in both horizon-

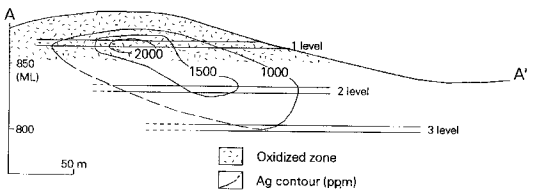

Fig. 2. Cross sections projected onto the planes of veins of the Oknam mine, showing the locations of silver-rich ore shoots and oxidized zone. For location see Fig. 1.

tal and vertical directions. They commonly branch into several thin veinlets. Quartz veins commonly containing angular wall-rock fragments consist mainly of massive fine-grained gray to white quartz with rare amounts of muscovite and sulfides. The sulfides occur mainly as thin layers at vein margins, and are disseminated throughout the vein. Around wall-rock breccia fragments, they also occur as successive crude bands.

Ag-Au-bearing rhodochrosite veins (No. 1 and No. 2 veins) can be traced up to 0.5 km, and have the thickness of $\leq$0.4 m (avg. 0.3 m). They commonly occur along the contact between earlier quartz veins and wall-rocks, and are often branched into several veinlets. Down to 20 to 30 m below the ground surface, rhodochrosites were strongly oxidized into manganese oxides (Fig. 2). The veins contain economic quantities of silver and gold with base-metal sulfides (mainly pyrite and arsenopyrite). Ore minerals mainly occur as massive sulfide bands at marginal portions of the vein. Sulfide minerals with rhythmic banding are also observed at intermediate vein portions. At the central vein portions, fine to coarse-grained sulfide minerals are disseminated. In vugs, rare amounts of fine-grained sulfide minerals occur.

No. 2 vein shows a systematic spatial variation in sulfide mineralogy in the ore shoots. Lateral mineral variation is more remarkable than vertical variation. General parageneses vary inwardly from the vein margin to the center as follows: arsenopyrite+pyrite $\Rightarrow$ sphalerite+chalcopyrite+galena+gold $\Rightarrow$ galena+Ag-bearing minerals. In upper (shallower) parts of the ore shoots, the veins contain relatively larger amounts of galena, sphalerite and silver minerals. The silver grade of the No. 2 vein varies with depth (Fig. 2). The grade in the oxidized zone is 16 to 146 g/ton Ag, whereas below the oxidized zone and down to level 2, silver is more enriched (689 to 4,501 g/ton Ag), implying that some silver was reprecipitated below the oxidized zone during the supergene process. Gold grade of the vein varies from 0.05 to 46.3 g/ton Au. However, gold is more concentrated in the silver-rich zone. Toward the lower (deeper) parts, the amounts of arsenopyrite becomes larger and exceeds those of pyrite. Ore sho- ots at Oknam show structural controls, and tend to be preferentially located at the places characterized by swelling and brecciation.

Wall-rocks were selectively altered by hydrothermal ore fluids especially during the quartz vein mineralization. Alteration zones have a maximum thickness of about 0.1 m, and are characterized by sericitic and carbonate assemblages. Phyllite was altered weakly to potassic and sericitic alteration assemblages with pyrites.

MINERALOGY AND PARAGENESIS

Polyascendant nature is a characteristic of the hydrothermal mineralization at Oknam. Mineralization stages and sequences were determined by vein textures such as crosscutting, brecciation, and lateral mineral zoning within a single vein (e.g., Kim, Nakamura, 1986). Hypogene open-space filling at Oknam is divided into five paragenetic stages. Each stage is separated from another by tectonic breaks characterized by faulting or fracturing (Fig. 3).

Stage I mineralization is represented by deposition of gray to white quartz, and contains minor amounts of pyrite, arsenopyrite, sphalerite and pyrrhotite. Gray quartz at vein margins is fine-grained with massive appearance, and is associated with muscovite. Fine-grained sulfide aggregates often occur as thin (<2 mm wide) layers at vein margins. Fine-grained anhedral pyrite occurs rarely as massive aggregates in marginal portions of the vein, whereas large euhedral pyrite crystals are rarely disseminated at center of the vein. Arsenopyrite (31.8 to 30.1 atomic% As) is intimately intergrown with pyrite. Fine-grained pyrrhotite and sphalerite (19.2 to 19.8 mol% FeS) are included in early pyrite. Following the brecciation of stage I vein, the introduction of stage II veins occurred.

Stage II and III mineralizations are characterized by the occurrence of manganese-bearing carbonates (predominantly rhodochrosite and rarely manganoan dolomite). During stage II mineralization, pink rhodochrosite and rare amounts of sulfides were precipitated together. Rhodochrosite is usually massive in appearance. Rare amounts of white calcite occurs in vugs as aggregates of small sheeted or rhombic crystals. Sulfides in stage II veins are predominantly pyrite and arsenopyrite which are intergrown each other especially at vein margins. Stage II rhodochrosite veins are cut by stage III veins.

Stage III rhodochrosite veins typically consists of three distinct bands (Fig. 3): dark pink band (early),

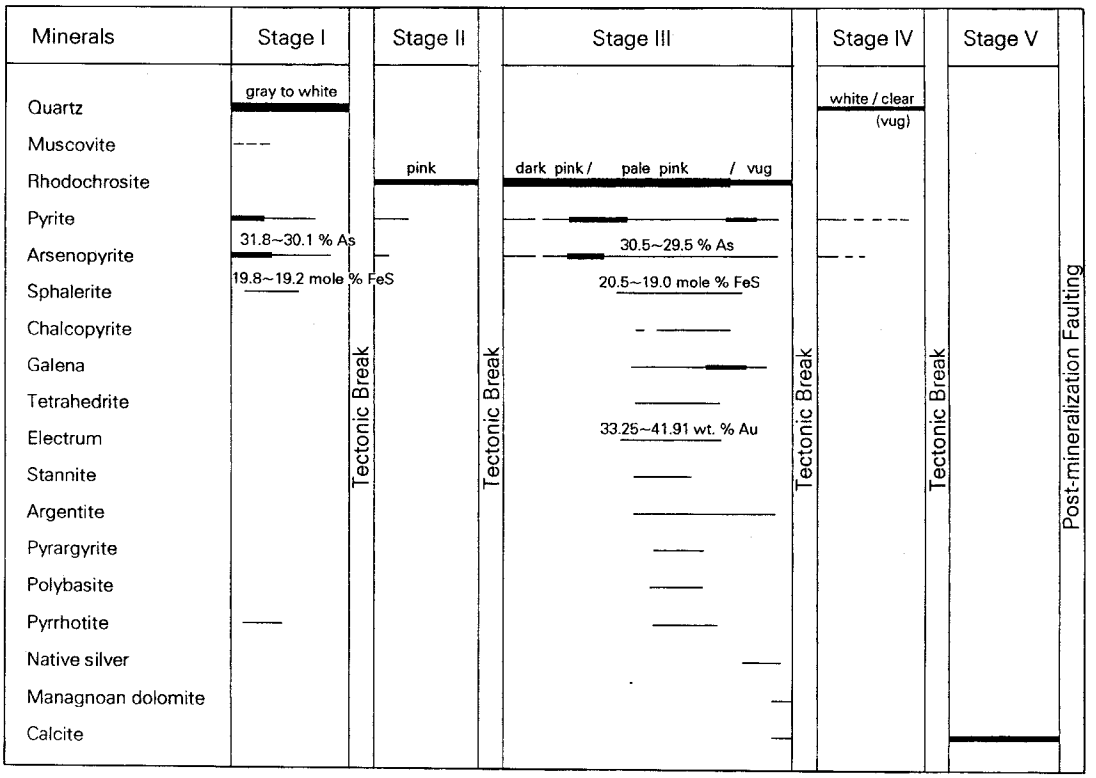

Fig. 3. Generalized paragenetic sequence of vein minerals from the Oknam Au-Ag mine. Chemical compositions of arsenopyrite (atom.% As), sphalerite (mole % FeS) and electrum (wt.% Au) are also shown. Width of lines corresponds to relative mineral abundance.

pale pink band (middle), and vug (late). The dark pink band is represented by the occurrence of dark pink rhodochrosite at marginal portions of the stage III vein. Very fine-grained pyrite and arsenopyrite are disseminated in this band. The pale pink band consists largely of reddish pink rhodochrosite at intermediate vein portions. Economic quantities of silver and gold, together with sulfide minerals, were deposited mainly in the pale pink band. Along the contact with the dark pink band, fine-grained pale pink rhodochrosite occurs as thin (<1 mm thick) layers. Pale pink rhodochrosite also occurs as euhedral overgrowths on central vugs. Manganoan dolomite and white calcite occur as aggregates in vugs of the stage III vein.

The pale pink band in stage III rhodochrosite veins contains abundant ore minerals such as arsenopyrite, pyrite, sphalerite, chalcopyrite, galena and rare amounts of tetrahedrite, pyrrhotite, pyrargyrite, polybasite, electrum, argentite, native silver and stannite. Pale pink rhodochrosite is the most abundant in the band, and usually occurs as medium- to coarse-grained transparent euhedral crystals. It also occurs as whitish pink translucent fine grains at the boundary with the dark pink band. At marginal (early) portions of the pale pink band, large amounts of arsenopyrite and pyrite occur as distinct mineralic bands. They were intensely fractured and cemented by later rhodochrosite with other sulfide minerals. Arsenopyrite and pyrite are also disseminated as fine-grained euhedral crystals at central vein portions. Pyrrhotite occurs as rounded inclusions in late pyrite and arsenopyrite, and is also intergrown with galena within sphalerite.

Anhedral dark brown sphalerite is often included within early pyrite in the pale pink band. Polycrystalline aggregates (each 0.5 to 0.8 cm in diameter) of sphalerite (19.0~20.5 mole.% FeS) mainly occur at intermediate to central vein portions. These sphalerites are also interstitial to the cataclastic pyrite and arsenopyrite, commonly replacing them along fractures and rims, and contain blebs of chalcopyrite. Sphalerite is often penetrated by late pyrite with lath shape.

Early chalcopyrite occurs as fine-grained euhedral crystals within the polycrystalline sphalerite aggregates in the pale pink band. Late chalcopyrite replaces the

sphalerite along cleavages and rims, or is interstitial to pyrite and arsenopyrite. Galena mostly occurs as fine to coarse-grained aggregates at intermediate to central portions of the pale pink band, and is closely associated with sphalerite.

At the central part of vein, fine-grained galena occurs as isolated grains within rhodochrosite matrix. Fine-grained anhedral tetrahedrite also occurs at central vein portions. It is often exsolved in galena but mainly replaces galena, pyrite and arsenopyrite. Tetrahedrite rarely crosscut the sphalerite, and infrequently contains tiny blebs of chalcopyrite and pyrargyrite.

Ag-bearing sulfosalts in stage III veins occur mainly as pyrargyrite and polybasite. They occur as inclusions in late pyrite, galena and tetrahedrite of the pale pink band, and are intimately intergrown each other. Electrum (33.25 to 41.91 wt.% Au) occurs mostly as tiny round grains in late sphalerite, pyrite and galena which fill the fractures of pyrite and arsenopyrite. Microscopic-sized argentite and stannite also occur in intermediate to central parts of stage III veins. Stannite occurs as irregular masses around and/or as inclusions in sphalerite. Argentite is commonly intergrown with stannite. It is also associated with native silver and calcite along the fractures of rhodochrosite. Native silver also rarely occurs as fine anhedral grains in galena.

Stage IV mineralization occurs as barren white quartz veins. During the latest mineralization (stage V), white calcite was deposited along fractures in earlier stage veins. The calcite is commonly fine-grained but also occurs as thin rhombic plates.

FLUID INCLUSIONS

Fluid inclusion studies were carried out on 29 samples (gray quartz, rhodochrosite and calcite) from the Oknam mine, in order to examine the spatial and temporal variations of temperature and composition of hydrothermal fluids. The samples cover broad areal extent of the productive vein: the horizontal extent of sampling is about 200 m, and the vertical extent is approximately 80 m. Microthermometric data of fluid inclusions were obtained on a FLUID INC. heating/freezing stage calibrated with synthetic CO_2 and H_2O inclusions. Temperature determinations were made on 593 inclusions, and salinity determinations on 129 inclusions (Figs. 4 and 5). No pressure corrections were made to the filling temperatures, as the evidence of periodic boiling indicates that the fluids trapped in primary inclusions mostly were on or close to the boiling point curve.

Minerals studied mostly contain numerous primary and secondary inclusions. However, secondary inclusions are more abundant. Two types of inclusions are recognized on the basis of their phase relations at room temperature: Type I and Type II. Type I inclusions contain a liquid and a vapor phase. The vapor usually makes up 5 to 20 percent of the total volume of inclusions. Type I inclusions are most abundant in all samples examined. No daughter minerals were observed in type I inclusions. They homogenize to the liquid phase upon heating. They are generally less than

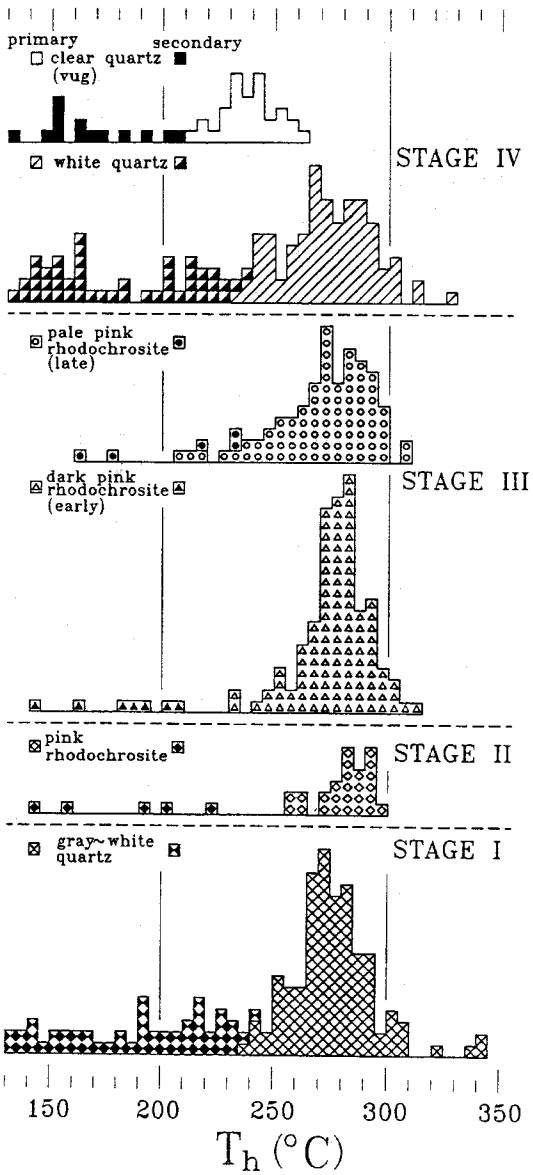

Fig. 4. Histograms showing homogenization temperatures of fluid inclusions in vein minerals from the Oknam Au-Ag mine.

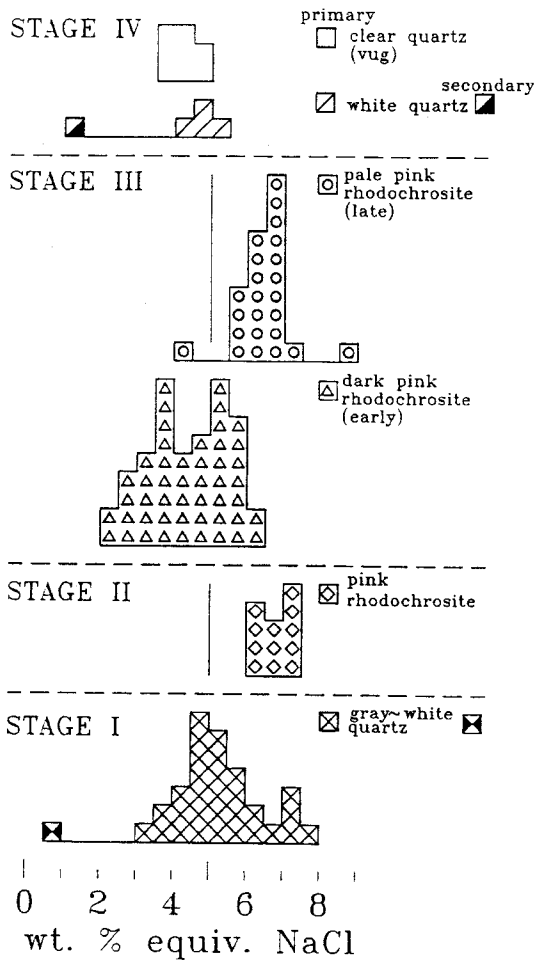

Fig. 5. Histograms of salinities of fluid inclusions in vein minerals from the Oknam Au-Ag mine.

20 μm (up to 50 μm in clear vug quartz) in diameter. Type II inclusions also contain a liquid and vapor phase, but the volume of vapor exceeds that of the liquid phase. They occur only as primary inclusions (generally less than 40 μm in size) and homogenize to the vapor phase upon heating.

Fluid inclusions in stage I mineralization

Gray to white quartz in stage I veins contains predominantly type I inclusions. Rare type II inclusions also occur in some samples from lower levels of the vein. Homogenization temperatures of primary fluid inclusions range from 240° to 345°C, but form a prominent cluster at temperatures between 260° and 290°C (Fig. 4). Within this range, type II inclusions homogenize at a narrow temperature range 280° to 285°C. Although most inclusions were not suitable for measurement of freezing temperatures because of their small size, measured salinities of primary type I inclusions range from 3.4 to 7.8 equiv. wt.% NaCl (Fig. 5).

Fluid inclusions in stage II and III mineralization

Both type I and type II fluid inclusions are observed in rhodochrosites from manganese-bearing carbonate stages (II and III). Homogenization temperatures of primary fluid inclusions in rhodochrosites from stages II and III veins range from 207° to 313°C, with a prominent peak at 250° to 300°C (Fig. 4).

Stage II pink rhodochrosite was not good for fluid inclusion study due to the rarity and small size of fluid inclusions. Measured homogenization temperatures of primary type I fluid inclusions range from 257° to 298°C. The salinity ranges from 6.2 to 7.4 equiv. wt.% NaCl (Figs. 4 and 5).

Rhodochrosites from stage III veins contain type I and rare type II inclusions. Measured homogenization temperatures for primary type I fluid inclusions range from 234° to 313°C for early dark pink rhodochrosite and from 207° to 306°C for late pale pink rhodochrosite. Salinity of primary inclusions range from 2.3 to 8.7 equiv. wt% NaCl (early dark pink rhodochrosite, 2.3 to 6.4; late pale pink rhodochrosite, 4.2 to 8.7 wt.%) (Figs. 4 and 5).

Fluid inclusions in stage IV mineralization

Massive white quartz and clear vug quartz from stage IV veins contains type I inclusions only. They homogenize at temperatures of 232° to 328°C (white quartz) and 213° to 264°C (clear vug quartz), and have salinities of 3.6 to 5.4 equiv. wt% NaCl (white quartz, 4.2 to 5.4; clear quartz, 3.6 to 4.8 wt.%) (Figs. 4 and 5).

Variation in temperature and composition of hydrothermal fluids

Homogenization temperature versus salinity plots of fluid inclusions in stage I quartz indicate the overall fluid history dominated by cooling and dilution (Fig. 6). However, both the recognized increase of salinity (up to 7.5 wt.% NaCl) of early stage I fluids at temperatures of 300°±10°C and the coexistence of type I and type II inclusions suggests the existence of boiling of early fluids. On the other hand, the salinity versus homogenization temperature diagrams for fluid inclusions in stage II and III rhodochrosites possibly indicate a complex history of cooling, dilution and

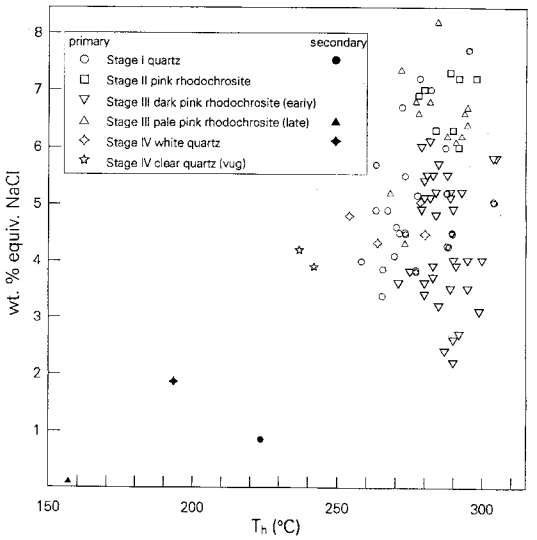

Fig. 6. Homogenization temperature versus salinity diagram for fluid inclusions in vein minerals from the Oknam Au-Ag mine.

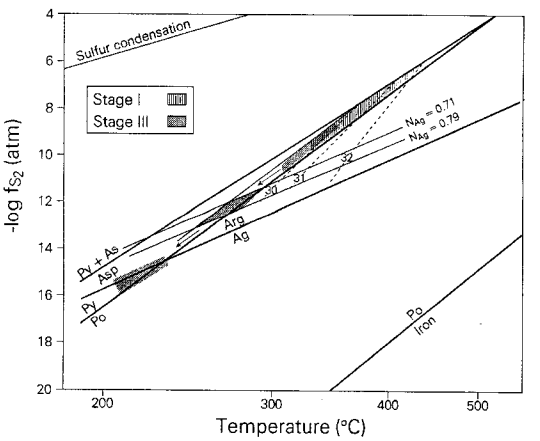

Fig. 7. Temperature versus sulfur fugacity diagram showing the possible conditions (dotted and hatched area) of mineralization in stages I and III of the Oknam mine. Short dashed lines are compositional isopleths (atomic % As) of arsenopyrite. N_{Ag} is the atomic fraction of Ag in electrum. Reaction curves from Clark (1960), Barton, Skinner (1979) and Barton, Toulmin (1964). Abbreviations: Ag; native silver, Arg; argentite, As; native arsenic, Asp; arsenopyrite, Po; pyrrhotite, Py; pyrite.

boiling of ore-forming fluids (Fig. 6). The relationship suggests that the deposition of abundant base-metal sulfides during stage III was mainly a consequence of the increase of salinity of ore fluids without no significant temperature change. The fluid boiling likely occurred as a result of pressure decrease by hydraulic(?) fracturing which formed especially during the transition from deposition of early dark pink band to late pale pink band in stage III, effectively resulting in deposition of abundant base-metal sulfides through destabilization of metal chloride complexes. During the stage IV mineralization, cooling and dilution of hydrothermal fluids occurred predominantly and resulted in a return to lower salinities.

Estimation of pressure conditions

The observed evidence of fluid boiling during stage I can be used to estimate the fluid pressures. Utilizing P-T-X data for H_2O-NaCl solutions (Sourirajan, Kennedy, 1962; Haas, 1971), the boiling of 5~7.5 wt.% NaCl fluid at temperatures of 300°±10°C indicates the fluid pressures falling in the range of about 90 to 340 bars. This pressure likely corresponds to maximum depths of about 300 and 1,200 m, assuming lithostatic and hydrostatic loads, respectively.

GEOCHEMICAL CONDITIONS OF ORE DEPOSITION

Data obtained from mineral assemblages and fluid inclusions have been utilized to trace the chemical evolution of mineral deposition at Oknam.

The presence of pyrite+arsenopyrite (30.1 to 31.8 atomic.% As)+sphalerite (19.2 to 19.8 mole.% FeS) assemblage in the early stage I mineralization restricts the fs_2 conditions to a narrow range (10^{-6} to 10^{-10} atm) at temperatures of about 300° to 400°C (Fig. 7).

Gold-silver-bearing rhodochrosite veins (stage III) show well-defined lateral mineralization sequence: early, pyrite+arsenopyrite assemblage in the dark pink band ⇒ middle, pyrite (pyrrhotite)+sphalerite+argentite+electrum assemblage in the pale pink band ⇒ late (vug), argentite+native silver assemblage with calcite. It is noteworthy that stage III arsenopyrites have the lower arsenic contents (29.5 to 30.5 atomic.% As) than stage I arsenopyrites. The pyrite+arsenopyrite assemblage defines the ranges of sulfur fugacity and formation temperature to about 10^{-6} to 10^{-10} atm and 310° to 360°C, respectively (Fig. 7).

The temperature and fs_2 ranges for the hydrothermal fluids during the deposition of middle, pyrite (pyrrhotite)+sphalerite+argentite+electrum assemblage in the pale pink band of stage III veins are estimated from phase relations in the system Au-Ag-S (Barton, Toulmin, 1964) and Fe-Zn-S (Toulmin, Barton, 1964; Scott, Barnes, 1971). Sphalerites coexisting with pyrite and pyrrhotite have the iron content of 19.0 to 20.5 mole % FeS. The silver contents of electrum coexisting with argentite range from 71 to 79 atomic

%. By applying an equation for temperature versus composition relationship to the electrum-sphalerite-pyrite-argentite assemblage (Shikazono, 1985), the probable temperature of formation is estimated to be about 240° to 300°C. The corresponding fs_2 values for this temperature range are about $10^{-11.5}$ to $10^{-13.5}$ atm (Fig. 7). During the late mineralization (near or in vugs) of stage III, argentite and native silver are in equilibrium with pyrite coexisting with pyrrhotite. Pyrrhotite disappears immediately during the calcite deposition in vugs. The maximum temperature and fs_2 values for the late stage III mineralization can be set by pyrite-pyrrhotite and argentite-native silver reaction curves. The maximum temperature is about 230°C, corresponding to a maximum fs_2 value of $10^{-14.5}$ atm (Fig. 7). Therefore, it is likely that stage III mineralization accompanied the systematic decreases of temperature and fs_2 with time.

Iron oxides were not observed in stage III veins. The maximum fo_2 condition for the pyrite+pyrrhotite assemblage which is common in stage III veins can be set by the triple point of the pyrite-pyrrhotite-magnetite reaction: $6FeS+2O_2=Fe_3O_4+3FeS_2$; log fo_2 (max.)=-1/2 log K. The estimated maximum fo_2 value for late to intermediate stage III fluids ($fs_2=10^{-13.6}$ atm and 250°C) is likely about 10^{-38} atm. The minimum fo_2 value also can be estimated to be 10^{-39} atm, based on the MnS-$MnCO_3$ reaction curve (Fig. 8).

Similarly, the possible stability ranges for the

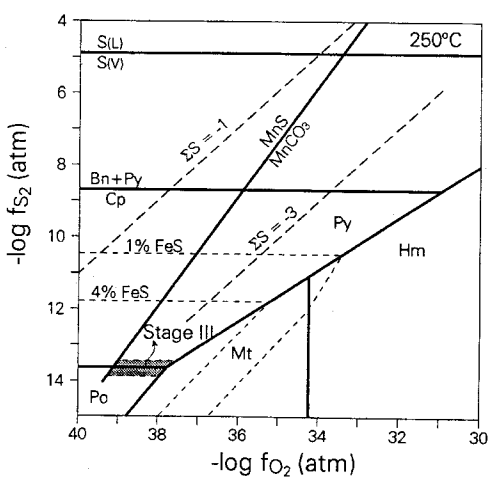

Fig. 8. Log fs_2 versus log fo_2 diagram at 250°C, showing the mineral stability fields for stage III mineralization (shaded area). The contours of FeS content indicate the deposition conditions of sphalerites. The estimated $m\Sigma S$ values range from $10^{-3.2}$ to $10^{-2.7}$ at fs_2 and fo_2 values of $10^{-13.5}$ and 10^{-38} to 10^{-39} atm, respectively. Abbreviations: Bn; bornite, Cp; chalcopyrite, Hm; hematite, Mt; magnetite, Po; pyrrhotite, Py; pyrite.

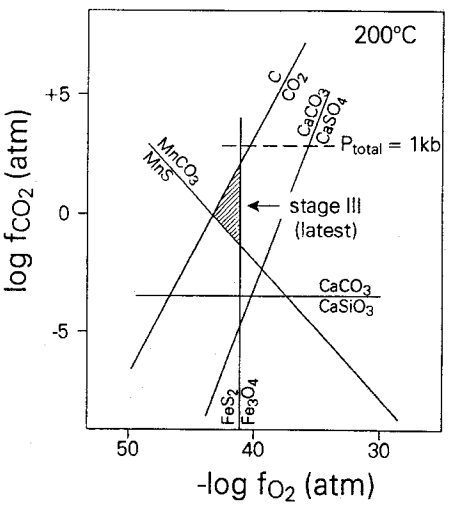

Fig. 9. Isothermal fo_2 versus fco_2 diagram at 200°C, showing phase relations of some systems. Shaded area indicates the depositional condition of the argentite+native silver assemblage in latest stage III mineralization. The pyrite/magnetite reaction curve at $fs_2=10^{-15.5}$ atm.

constituents in the latest stage III mineralization near or in vugs can be shown on the isothermal fo_2-fco_2 diagram at 200°C (Fig. 9). The reactions used are as follows: $C+O_2=CO_2$; $MnS+CO_2+1/2O_2=MnCO_3+1/2S_2$; $CaCO_3+SiO_2=CaSiO_3+CO_2$; $Fe_3O_4+3S_2=3FeS_2+2O_2$; $CaSO_4+CO_2=CaCO_3+1/2S_2+3/2O_2$.

Graphite and alabandite were not found in the latest stage III mineralization and, therefore, the rhodochrosite+alabandite and $C+CO_2$ reaction curves define a lower limit of fo_2. Based on the absence of iron oxides, pyrite+magnetite reaction curve at $fs_2=10^{-15}$ atm also defines the upper limit of fo_2. Accordingly, the probable fo_2 range is about $10^{-41.5}$ to $10^{-43.5}$ atm at 200°C (Fig. 9).

The pH of the hydrothermal fluids that travelled through host rocks was probably controlled by the assemblage quartz+mica+feldspar in rocks. The pH of a solution containing 10^{-1} to 10^{-2} moles/kg of K^+, in equilibrium with the assemblage K-feldspar+muscovite+quartz, is calculated to be about 5.1 to 6.1 at 250°C (Fig. 10). If the hydrothermal fluids later equilibrated with calcite, however, the pH would be controlled by the dissolution of calcite. Pure water in equilibrium with calcite at 200°C (for the latest stage III) would have a pH up to about 7.5 (Fig. 11).

Under the pH conditions below neutrality, pyrrhotite occurs predominantly where H_2S is the predominant sulfur species ($mH_2S=m\Sigma S$) in the system. Then, the molality of total sulfur ($m\Sigma S$) can be calculated from an equation $H_2S(aq)+FeS+1/2O_2=FeS_2+$

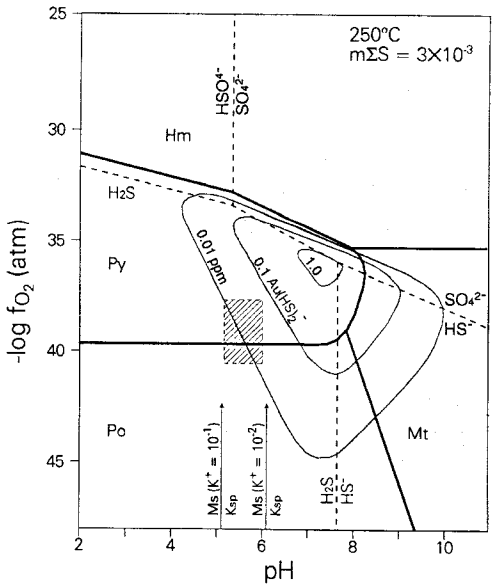

Fig. 10. Mineral and sulfur species diagram in terms of pH and fo_2, showing the solubilities of gold (in mg/kg as a bisulfide complex) at 250°C and $m\Sigma S=3\times10^{-3}$. Shaded area indicates the condition of the mineral assemblage in late stage III veins at Oknam. Abbreviations: Hm; hematite, Ksp; K-feldspar, Ms; muscovite, Mt; magnetite, Po; pyrrhotite, Py; pyrite.

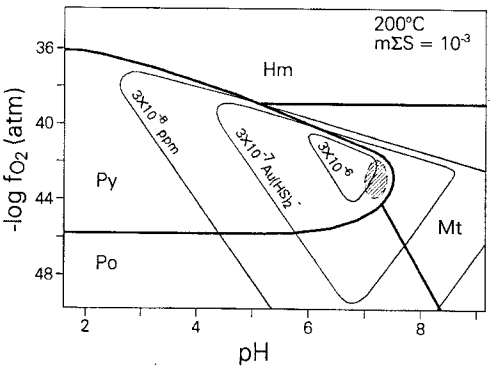

Fig. 11. Log fo_2 versus pH diagram showing the solubility of $Au(HS)_2^-$ at 200°C and $m\Sigma S=10^{-3}$. Shaded area indicates the chemistry of hydrothermal fluids for the latest stage III mineralization at Oknam. Abbreviations: Hm; hematite, Mt; magnetite, Po; pyrrhotite, Py; pyrite.

H_2O (aq). For this reaction, log mH_2S value equals to -(1/2 log fo_2+log K-log γ_{H_2S}), where γ_{H_2S} is the activity coefficient of H_2S. Therefore, the total sulfur concentrations ($m\Sigma S$) for the pyrite+pyrrhotite coexistence during the intermediate to late stage III mineralization are approximately calculated to be $10^{-2.7}$ to $10^{-3.2}$ m at 250°C and fo_2 values of 10^{-38} to 10^{-39} atm (see Fig. 8).

Previous studies have shown that either chloride or bisulfide complexes are the most important transport agents for gold. Transportation as bisulfide complexes is favored for low-temperature, low-salinity fluids. Therefore, the evaluation of bisulfide complexing was performed to elucidate the mechanism(s) of gold precipitation at Oknam. Utilizing the solubility data of Seward (1973) for bisulfide complexing, the gold solubility in stage III fluids was evaluated. The calculated gold solubility dropped greatly as the fluid cooled from 250°C to 200°C (Figs. 10 and 11): at 250°C, $fo_2=10^{-38}$ to 10^{-39} atm, and pH=5.1 to 6.1, calculated gold solubility=10^{-2} to 10^{-1} ppm; at 200°C, $fo_2=10^{-41.5}$ to $10^{-43.5}$, and pH=7.5, calculated gold solubility=3×10^{-6} ppm. Therefore, it is likely that gold deposition at Oknam occurred as a combined result of a rise in pH and drops in fo_2 and temperature.

ACKNOWLEDGEMENTS

This study was financially supported by the academic research fund of Ministry of Education, Republic of Korea. Fluid inclusion studies were supported in part by the Center for Mineral Resources Research (CMR), Korea University.

REFERENCES

Barton, P.B., Jr. and Skinner, B.J. (1979) Sulfide mineral stabilities. In: Geochemistry of hydrothermal ore deposits (Barnes, H.L., ed.), New York, Wiley and Sons Pub. Co. p. 278-430.

Barton, P.B., Jr. and Toulmin, P., III (1964) The electrum tarnish method for determination of the fugacity of sulfur in laboratory sulfide systems. Geochim. Cosmochim. Acta, v. 28, p. 619-640.

Barton, P.B., Jr. and Toulmin, P., III (1966) Phase relations involving sphalerite in the Fe-Zn-S system. Econ. Geol., v. 61, p. 815-849.

Choo, S.H. and Kim, S.J. (1985) A study of Rb-Sr age determinations on the Ryeongnam Massif (I) : Pyeonghae, Buncheon and Kimcheon granite gneisses. KIER Annual Report 85-24, p. 7-39 (in Korean).

Clark, L.A. (1960) The Fe-As-S system: phase relations and applications. Econ. Geol., v. 55, p. 1345-1381 and 1631-1652.

Haas, J.L., Jr. (1971) The effect of a hydrothermal system at hydrostatic pressure. Econ. Geol., v. 66, p. 940-946.

Imai, N. and Lee, H.K. (1980) Complex sulphide-sulphosalt ores from Janggun mine, Republic of Korea. In: Complex sulphide ores (Proc. Inter. Conf. for Complex Sulphide Ores), Rome, Oct. 5-8, p. 248-259.

Kim, K.H. (1986) Origin of manganese carbonates in the Janggun mine, South Korea. Jour. Korean Inst. Mining Geol., v. 19, p. 109-122.

Kim, K.H. and Nakai, N. (1980) Carbon and oxygen isotope studies of the carbonate rocks from the Synyemi zinc-lead ore deposits, western Taebaegsan metallogenic belt, Korea. Nagoya Univ. [Japan], Jour. Earth Sci., v. 28, p. 57-74.

Kim, K.H., Nakai, N. and Kim, O.J. (1981) A mineralogical study of the skarn minerals from the Shinyemi lead-zinc ore deposits, Korea. Jour. Korean Inst. Mining Geol., v. 14, p. 167-182.

Kim, M.Y. and Nakamura, T. (1986) Some problems on the concept of mineral paragenesis and macrostructures of ore veins, with special reference to those of ore veins at the Ohtani mine, Kyoto Prefecture, Japan. Jour. Korean Inst. Mining Geol., v. 19, Spec. Iss., p. 97-102 (in Korean).

Kim, O.J., Hong, M.S., Kim, K.T. and Park, H.I. (1962) Geological Map of Korea, 1:50,000 Samgeun-ri Sheet, Geological Survey of Korea.

Koh, Y.K., Choi, S.G., So, C.S., Choi, S.H. and Uchida, E. (1992) Application of arsenopyrite geothermometry and sphalerite geobarometry to the Taebaek Pb-Zn(-Ag) deposit at the Yeonhwa I mine, Republic of Korea. Mineralium Deposita, v. 27, p. 58-65.

Lee, H.K., Ko, S.J. and Imai, N. (1990) Genesis of the lead-zinc-silver and iron deposits of the Janggun mine as related to their structural features : Structural control and wall rock alteration of ore-formation. Jour. Korean Inst. Mining Geol., v. 23, p. 161-181.

Scott, S.D. and Barnes, H.L. (1971) Sphalerite geothermometry and geobarometry. Econ. Geol., v. 66, p. 653-669.

Seward, T.M. (1973) Thio complexes of gold and the transport of gold in hydrothermal ore solutions. Geochim. Cosmochim. Acta, v. 37, p. 337-399.

Shelton, K.L., So, C.S. and Chang, J.S. (1988) Gold-rich mesothermal vein deposits of the Republic of Korea : Geochemical studies of the Jungwon gold area. Econ. Geol., v. 83, p. 1221-1237.

Shikazono, N. (1985) A comparison of temperature estimated from the electrum-sphalerite-pyrite-argentite assemblage and filling temperatures of fluid inclusions from epithermal Au-Ag vein-type deposits in Japan. Econ. Geol., v. 80, p. 1415-1424.

So, C.S., Yun, S.T. and Chi, S.J. (1989) Geochemical studies of hydrothermal gold-silver deposits, Republic of Korea : Yangdong mining district. Jour. Geol. Soc. Korea, v. 25, p. 16-29.

So, C.S., Yun, S.T. and Koh, Y.K. (1993) Mineralogic, fluid inclusion, and stable isotope evidence for the genesis of carbonate-hosted Pb-Zn(-Ag) orebodies of the Taebaek deposit, Republic of Korea. Econ. Geol., v. 88, p. 855-872.

Sourirajan, S. and Kennedy, G.C. (1962) The system H_2O-NaCl at elevated temperatures and pressures. Amer. J. Sci., v. 260, p. 115-141.

Toulmin, P.III, and Barton, P.B., Jr. (1964) A thermodynamic study of pyrite and pyrrhotite. Geochim. Cosmochim. Acta, v. 28, p. 641-671.

Ueda, N. (1968) Evolution of the continent in northeastern Asia. I: Reconnaisance survey of the geochronology of the Korean peninsula. Ms. Thesis, Dept. Geol., Univ. Tokyo, Japan.

Yang, D.Y., Utsugi, Y. and Mariko, T. (1993) Fluid inclusion study on magnesian Fe skarn-type deposit of the Shinyemi mine, Republic of Korea. Resource Geology, v. 43, p. 11-22.

Yun, S. (1979) Structural and compositional characteristics of skarn zinc-lead deposits in the Yeonhwa-Ulchin mining district, southeastern Taebaegsan region, Korea, Part I : The Yeonhwa I mine. Jour. Korean Inst. Mining Geol., v. 12, p. 51-73.

1998년 7월 14일 원고접수, 9월 11일 게재승인.

북부 소백산 육괴 지역에 부존하는 옥남 광산의 열수 금-은 광화작용

윤성택 · 지세정 · 소칠섭 · 허철호

요 약 : 옥남 금-은 광상은 소백산육괴 선캠브리아기 율리층의 흑운모편암 및 천매암 내에 발달하는 함금-은 능망간석맥으로 산출된다. 광맥의 상호 구조에 근거하여 5회의 광물 침전기(stage)가 인지되며, 각 시기는 특징적인 광물 조합을 나타낸다. 함금-은 맥(광화 3기)에서의 정출 광물은 맥의 연변부로부터 내측으로 가면서 다음과 같이 변화한다: 유비철석+황철석 (암색 능망간석 밴드 내) ⇒ 섬아연석+황동석+방연석+에렉트럼 (담색 능망간석 밴드 내) ⇒ 방연석+함은 광물 (정동 부위). 유체포유물 자료에 의하면, 광화유체의 온도 및 염농도는 시간에 따라 전반적으로 다음과 같이 감소했음을 지시한다: 광화 I기 (석영맥 광화작용), 345°~240°C, 3.4~7.8 wt.% NaCl 상당농도; 함망간 탄산염기 (II 및 III), 313°~207°C, 2.3~8.7 wt.% NaCl; 광화 4기 (석영맥 광화작용), 328°~213°C, 3.6~5.4 wt.% NaCl. 광화유체는 냉각 · 희석 상태의 순환강우의 혼입과 주기적으로 반복된 비등을 통하여 진화한 것으로 사료되며, 유체포유물 자료와 지질 증거에 의하면 광화작용 중 압력은 90~340 bar이었다. 금은 함은량이 높은 에렉트럼 (21~29 atom.% Au)으로 산출되며, 주로 300°~240°C 사이의 온도에서 침전되었다. 열역학적 검토에 의하면, 금은 pH의 증가와 더불어 온도, 유황분압 및 산소분압의 감소에 의해 침전하였으리라 사료된다.